

Enhanced Electrochemical Performance of Si-doped LiMn_2O_4 Cathode Material for LiBs Prepared using Mn_3O_4 Octahedrons

Gan Zhu¹, Mingze Qin¹, Tingting Wu^{*}, Mengyuan Zhao, Yansheng Shen, Yu Zhou, Yue Su, Yunhang Liu, Meimei Guo, Yongfeng Li, Hongyuan Zhao^{*}

Research Center for Advanced Materials and Electrochemical Technology, School of Mechanical and Electrical Engineering, Henan Institute of Science and Technology, Xinxiang 453003, China

*E-mail: wtingtingwu@163.com (T. Wu), hongyuanzhao@126.com (H. Zhao)

Received: 8 March 2022 / Accepted: 28 March 2022 / Published: 5 April 2022

We proposed a co-modification strategy of Si-doping and octahedral morphology to improve the electrochemical performance of LiMn_2O_4 . The Si-doped LiMn_2O_4 sample ($\text{LiSi}_{0.05}\text{Mn}_{1.95}\text{O}_4$ octahedrons) was prepared by high-temperature solid-state method with Mn_3O_4 octahedrons as manganese precursor and SiO_2 nanoparticles as silicon dopant. XRD and SEM characterization results indicated that the introduction of Si^{4+} ions does not produce the substantive impact on the inherent spinel structure of LiMn_2O_4 and $\text{LiSi}_{0.05}\text{Mn}_{1.95}\text{O}_4$ octahedrons present relatively uniform particle size distribution. When cycled at 1.0 C, $\text{LiSi}_{0.05}\text{Mn}_{1.95}\text{O}_4$ octahedrons exhibited higher initial reversible capacity than that of the undoped LiMn_2O_4 . After 100 cycles, $\text{LiSi}_{0.05}\text{Mn}_{1.95}\text{O}_4$ octahedrons showed better cycling stability with higher capacity retention rate of 94.7%. Moreover, $\text{LiSi}_{0.05}\text{Mn}_{1.95}\text{O}_4$ octahedrons presented good rate capability and high-temperature cycling performance. Such good electrochemical performance has much to do with the synergistic modification of Si-doping and octahedral morphology.

Keywords: LiMn_2O_4 ; Silicon doping; Octahedral morphology; Mn_3O_4 octahedrons; Electrochemical performance

1. INTRODUCTION

Lithium manganate oxide (LiMn_2O_4) is very important cathode material for lithium-ion batteries (LiBs). Compared with other commercial cathode materials, LiMn_2O_4 possesses several advantages such as high voltage platform, abundant manganese resource, and low production cost, which promote the widespread use of LiMn_2O_4 in the field of energy storage and low-speed electric vehicles [1-6]. However, the poor cycling performance of LiMn_2O_4 seriously affects the large-scale application of this cathode material to some extent.

To enhance the cycling performance, many scientific researchers optimized the electrochemical performance of LiMn_2O_4 by using several modification strategies such as doping modification [7-15],

surface coating, controlling nanoparticles granularity, and so on. Among these strategies, the doping modification performs an important role in enhancing the electrochemical performance of LiMn_2O_4 . The doping ions mainly involve the low valent cations (Cu^{2+} , Mg^{2+} , Al^{3+}) [3, 11, 16], high valent cations (Si^{4+} , Ti^{4+}) [17-19]. Among them, the high valent cations mainly replace the tetravalent manganese ions, which can avoid the decrease of reversible capacity [5, 18]. It has been reported that the Si-doping strategy can contribute to the increase of reversible capacity and improvement of cycling stability [17, 20]. Iturrondobertia reported the preparation of Si-doped LiMn_2O_4 by freeze-drying method [17]. Compared with the undoped spinel, the Si-doped LiMn_2O_4 sample presented a higher initial discharge capacity with better cycling stability. Zhao prepared the $\text{LiSi}_x\text{Mn}_{2-x}\text{O}_4$ samples by using electrolytic manganese dioxide (EMD) as manganese precursor and tetraethylorthosilicate as silicon dopant [20]. These research works indicate that a certain amount of silicon ions can effectively enhance the electrochemical performance of LiMn_2O_4 .

In this work, the $\text{LiSi}_{0.05}\text{Mn}_{1.95}\text{O}_4$ octahedrons were prepared by high-temperature solid-state method with Mn_3O_4 octahedrons as manganese precursor and SiO_2 nanoparticles as silicon dopant. Compared with the undoped LiMn_2O_4 , the introduction of Si^{4+} ions does not produce the substantive impact on the inherent spinel structure of LiMn_2O_4 . Electrochemical testing shows that the $\text{LiSi}_{0.05}\text{Mn}_{1.95}\text{O}_4$ octahedrons showed good electrochemical performance.

2. EXPERIMENTAL

To prepare the Si-doped LiMn_2O_4 sample, Mn_3O_4 octahedrons and SiO_2 nanoparticles were applied as manganese precursor and silicon dopant. The $\text{LiSi}_{0.05}\text{Mn}_{1.95}\text{O}_4$ octahedrons were prepared by high-temperature solid-state method. First of all, Mn_3O_4 octahedrons were prepared by hydrothermal method according to the previous work [21]. A certain amount of potassium permanganate (KMnO_4 , 4.5 g) and ethylene glycol ($\text{C}_2\text{H}_6\text{O}_2$, 7.5 ml) were dissolved successively in deionized water (100 ml). The obtained suspension was sealed in 150 ml Teflon-lined stainless steel autoclave and then maintained at 150 °C for 20 h. Based on the hydrothermal reaction process, Mn_3O_4 octahedrons were obtained by suction filtration and dried at 80 °C for 15 h. And then, the stoichiometric mixture of $\text{LiOH}\cdot\text{H}_2\text{O}$, SiO_2 nanoparticles, and Mn_3O_4 octahedrons were thoroughly mixed with the help of ethanol. Finally, the obtained mixture was sintered at 780 °C for 10 h in muffle furnace. By contrast, both the undoped LiMn_2O_4 and $\text{LiSi}_{0.05}\text{Mn}_{1.95}\text{O}_4$ particles were prepared through the similar solid state reaction process with electrolytic MnO_2 as manganese precursor.

The microstructures and surface morphologies of the undoped LiMn_2O_4 particles, $\text{LiSi}_{0.05}\text{Mn}_{1.95}\text{O}_4$ particles, and $\text{LiSi}_{0.05}\text{Mn}_{1.95}\text{O}_4$ octahedrons were characterized by X-ray diffraction (XRD) and scanning electron microscope (SEM). XRD pattern was used to confirm the influence of Si-doping on the microstructure of LiMn_2O_4 , and SEM image was applied to study the influence of Si-doping on the surface morphology of LiMn_2O_4 . The electrochemical performance of the undoped LiMn_2O_4 particles, $\text{LiSi}_{0.05}\text{Mn}_{1.95}\text{O}_4$ particles, and $\text{LiSi}_{0.05}\text{Mn}_{1.95}\text{O}_4$ octahedrons were tested by LANHE CT2001A battery tester.

3. RESULTS AND DISCUSSION

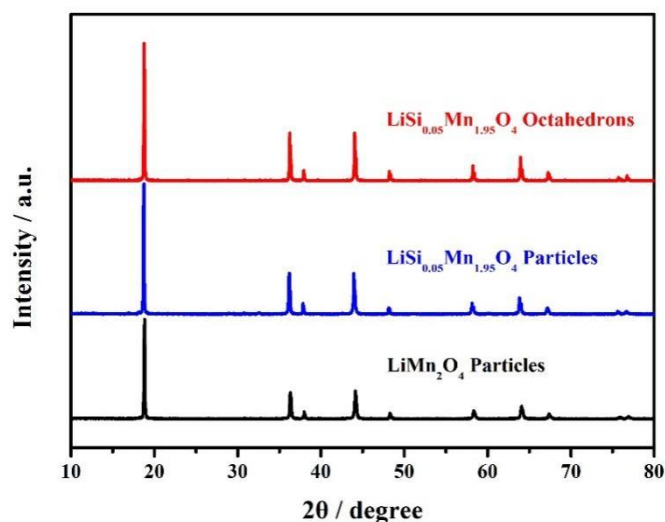


Figure 1. XRD patterns of (a) LiMn₂O₄ particles, (b) LiSi_{0.05}Mn_{1.95}O₄ particles, and (c) LiSi_{0.05}Mn_{1.95}O₄ octahedrons.

Figure 1 shows the XRD patterns of the undoped LiMn₂O₄ particles, LiSi_{0.05}Mn_{1.95}O₄ particles, and LiSi_{0.05}Mn_{1.95}O₄ octahedrons. As shown here, both LiMn₂O₄ particles and LiSi_{0.05}Mn_{1.95}O₄ particles present obvious characteristic diffraction peaks of LiMn₂O₄ (JCPDS No. 35-0782) [12, 22].

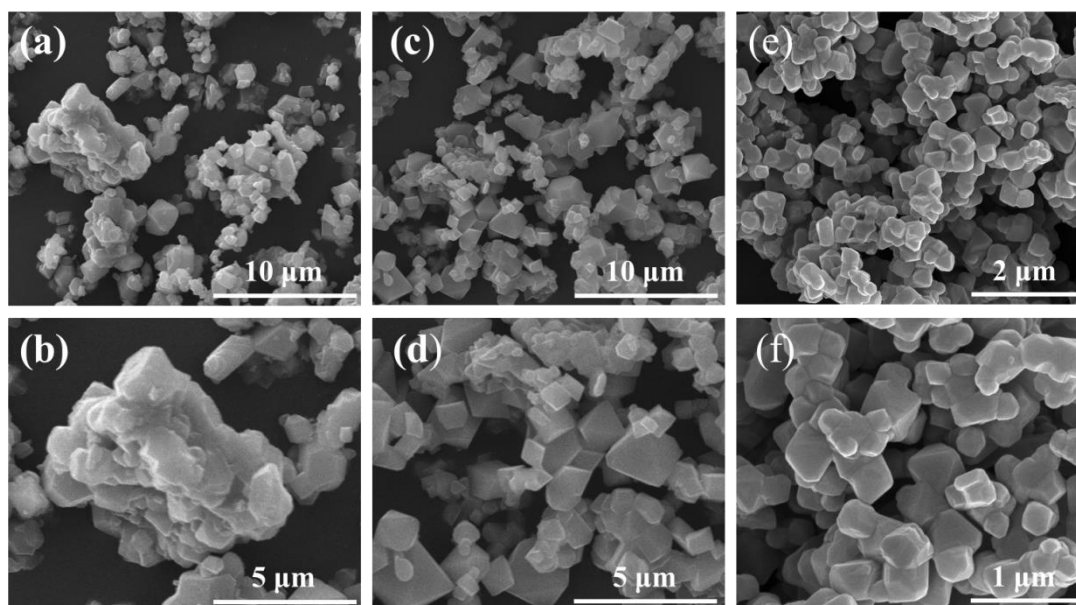


Figure 2. SEM images of (a, b) LiMn₂O₄ particles, (c, d) LiSi_{0.05}Mn_{1.95}O₄ particles, and (e, f) LiSi_{0.05}Mn_{1.95}O₄ octahedrons.

No other impurity peaks of MnO₂ or SiO₂ can be observed in the above XRD patterns, which suggests the successful transformation of electrolytic MnO₂ to LiMn₂O₄ and integration of Si⁴⁺ ions in the crystal structure of LiMn₂O₄ [20]. For the LiSi_{0.05}Mn_{1.95}O₄ octahedrons, the corresponding XRD

pattern shows similar characteristic diffraction peaks of LiMn_2O_4 without any other impurity peaks of Mn_3O_4 and SiO_2 , which indicates that Mn_3O_4 octahedrons were completely converted to the $\text{LiSi}_{0.05}\text{Mn}_{1.95}\text{O}_4$ sample [21, 23]. Furthermore, there is no (220) peak in the above XRD patterns of $\text{LiSi}_{0.05}\text{Mn}_{1.95}\text{O}_4$ particles and $\text{LiSi}_{0.05}\text{Mn}_{1.95}\text{O}_4$ octahedrons. It has been reported that the emergence of (220) peak means the colonization of doped cations at tetrahedral (8a) sites [13, 24]. Thus, it can be inferred that Si^{4+} ions only replace Mn^{4+} ions at octahedral (16d) sites, which can enhance the spinel structural stability.

Figure 2 shows the SEM images of the undoped LiMn_2O_4 particles, $\text{LiSi}_{0.05}\text{Mn}_{1.95}\text{O}_4$ particles, and $\text{LiSi}_{0.05}\text{Mn}_{1.95}\text{O}_4$ octahedrons. It can be seen from Figure 2(a, b) that the undoped LiMn_2O_4 particles show uneven particle size distribution. Some large agglomerated particles can be observed in the above SEM images. By contrast, the $\text{LiSi}_{0.05}\text{Mn}_{1.95}\text{O}_4$ particles shown in Figure 2(c, d) present relatively uniform particle size distribution, which has much to do with the introduction of Si^{4+} ions [17, 20]. The introduction of Si^{4+} ions contributes to the inhibition of large agglomerated particles, and the Si-doped LiMn_2O_4 sample can present uniform particle size distribution compared to the undoped LiMn_2O_4 particles. It should be noted that the $\text{LiSi}_{0.05}\text{Mn}_{1.95}\text{O}_4$ particles shown in Figure 2(c, d) also possess octahedral morphology. However, the corresponding particle size range is larger than that of $\text{LiSi}_{0.05}\text{Mn}_{1.95}\text{O}_4$ octahedrons shown in Figure 2(e, f). For the $\text{LiSi}_{0.05}\text{Mn}_{1.95}\text{O}_4$ octahedrons, the particle size distribution is completely different from that of the undoped LiMn_2O_4 particles and $\text{LiSi}_{0.05}\text{Mn}_{1.95}\text{O}_4$ particles. The obtained $\text{LiSi}_{0.05}\text{Mn}_{1.95}\text{O}_4$ octahedrons present uniform particle size distribution with smaller particle size, which may enhance the electrochemical performance of LiMn_2O_4 .

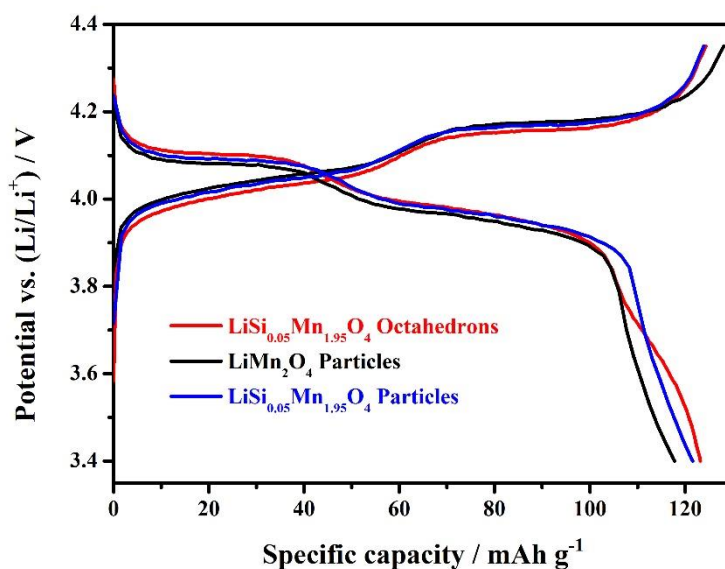


Figure 3. Initial charge-discharge curves of the undoped LiMn_2O_4 particles, $\text{LiSi}_{0.05}\text{Mn}_{1.95}\text{O}_4$ particles, and $\text{LiSi}_{0.05}\text{Mn}_{1.95}\text{O}_4$ octahedrons.

Figure 3 shows the initial charge-discharge curves of the undoped LiMn_2O_4 particles, $\text{LiSi}_{0.05}\text{Mn}_{1.95}\text{O}_4$ particles, and $\text{LiSi}_{0.05}\text{Mn}_{1.95}\text{O}_4$ octahedrons. These three samples were cycled at 0.5 C under the room temperature environment. It can be clearly observed that there are two obvious voltage platforms in the initial discharge curves of the undoped LiMn_2O_4 particles. For the $\text{LiSi}_{0.05}\text{Mn}_{1.95}\text{O}_4$ particles and $\text{LiSi}_{0.05}\text{Mn}_{1.95}\text{O}_4$ octahedrons, the corresponding voltage platforms coincide quite well with that of the undoped LiMn_2O_4 particles, which suggests that the introduction of Si^{4+} ions does not change the lithium intercalation process of electrochemical cycling [17, 20].

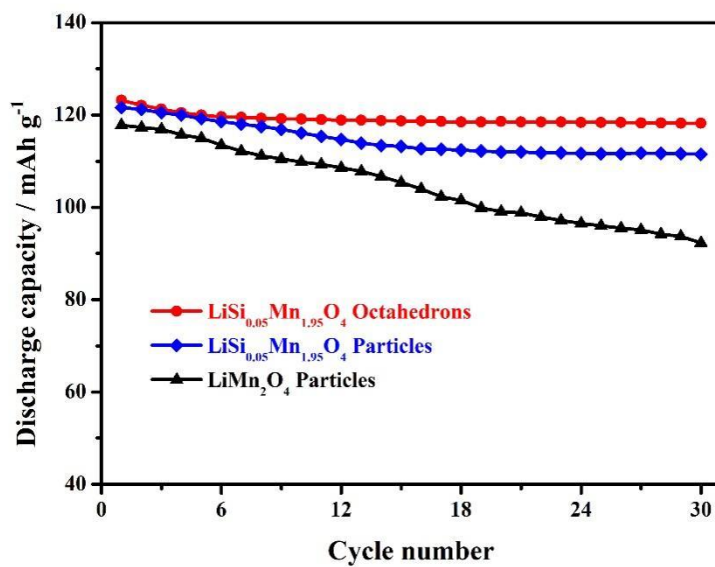


Figure 4. Cycling performance of the undoped LiMn_2O_4 particles, $\text{LiSi}_{0.05}\text{Mn}_{1.95}\text{O}_4$ particles, $\text{LiSi}_{0.05}\text{Mn}_{1.95}\text{O}_4$ octahedrons at 0.5 C.

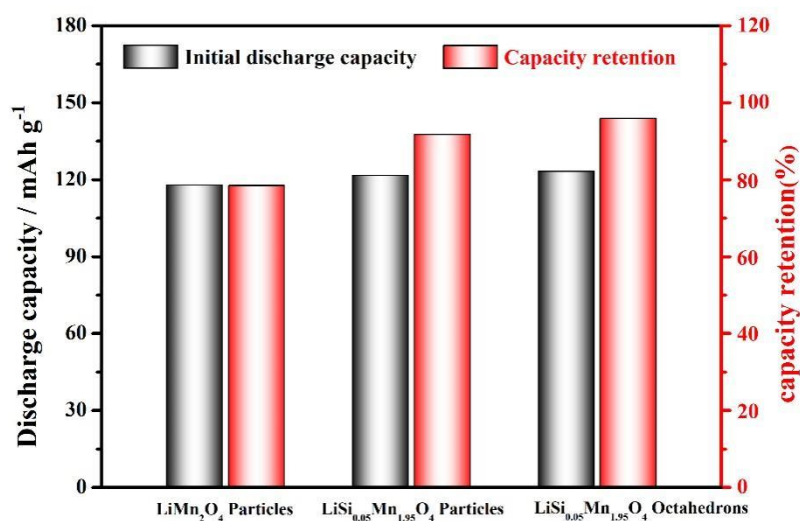


Figure 5. Histogram comparison of initial discharge capacity and capacity retention of the undoped LiMn_2O_4 particles, $\text{LiSi}_{0.05}\text{Mn}_{1.95}\text{O}_4$ particles, $\text{LiSi}_{0.05}\text{Mn}_{1.95}\text{O}_4$ octahedrons at 0.5 C.

Figure 4 presents the cycling performance of the undoped LiMn_2O_4 particles, $\text{LiSi}_{0.05}\text{Mn}_{1.95}\text{O}_4$ particles, $\text{LiSi}_{0.05}\text{Mn}_{1.95}\text{O}_4$ octahedrons at 0.5 C. It can be seen that the undoped LiMn_2O_4 particles exhibit poor cycling stability with low capacity retention rate of 78.4%. For the Si-doped LiMn_2O_4 samples, both $\text{LiSi}_{0.05}\text{Mn}_{1.95}\text{O}_4$ particles and $\text{LiSi}_{0.05}\text{Mn}_{1.95}\text{O}_4$ octahedrons show relatively better cycling stability (91.7% and 95.9%) compared to the undoped LiMn_2O_4 particles. Especially, the $\text{LiSi}_{0.05}\text{Mn}_{1.95}\text{O}_4$ octahedrons exhibit the best cycling stability with highest initial discharge capacity of 123.2 mAh g^{-1} and capacity retention. The change trend of initial discharge capacity and capacity retention of these three samples can be intuitively observed by Figure 5. Compared with the undoped LiMn_2O_4 particles, the good electrochemical performance is intimately connected to the co-modification of Si-doping and octahedral morphology of $\text{LiSi}_{0.05}\text{Mn}_{1.95}\text{O}_4$ octahedrons with uniform particle size distribution [17, 23, 25].

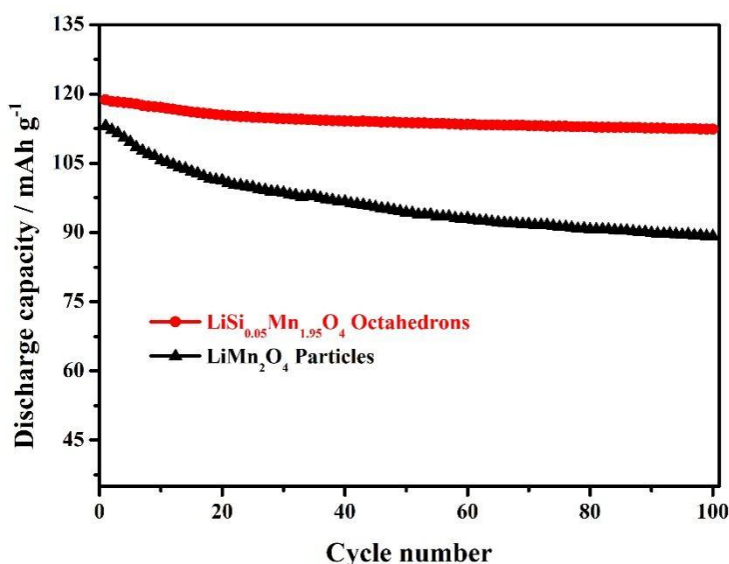


Figure 6. Long cycling performance of the undoped LiMn_2O_4 particles and $\text{LiSi}_{0.05}\text{Mn}_{1.95}\text{O}_4$ octahedrons at 1.0 C.

Figure 6 shows the long cycling performance of the undoped LiMn_2O_4 particles and $\text{LiSi}_{0.05}\text{Mn}_{1.95}\text{O}_4$ octahedrons at 1.0 C. The undoped LiMn_2O_4 particles show an initial discharge capacity of 113.1 mAh g^{-1} . With the increasing of cycling number, the discharge capacity presents a severe attenuation with relatively low retention rate of 75.3% after 100 cycles. For the Si-doped LiMn_2O_4 sample, $\text{LiSi}_{0.05}\text{Mn}_{1.95}\text{O}_4$ octahedrons show relatively good electrochemical performance due to the co-modification of Si-doping and octahedral morphology [17, 21, 23]. The initial discharge capacity of $\text{LiSi}_{0.05}\text{Mn}_{1.95}\text{O}_4$ octahedrons reach up to 118.7 mAh g^{-1} . After 100 cycles, the corresponding capacity retention increases to 94.7%. Such good electrochemical performance has much to do with the synergistic effect of Si-doping and octahedral morphology. Table 1 Comparison of $\text{LiSi}_{0.05}\text{Mn}_{1.95}\text{O}_4$ octahedrons and LiMn_2O_4 -based cathode materials reported by other works. The comparison result can further confirm the positive role of Si-doping and octahedral morphology. Compared with the undoped LiMn_2O_4 nanoparticles, the Si-doped LiMn_2O_4 sample can show higher initial discharge capacity, and

the octahedral morphology can enhance the cycling stability of LiMn_2O_4 . The Si-doping can provide the more expanded and regular MnO_6 octahedra, which achieves the better accommodation of Mn(III)–Mn(IV) interconversion during the electrochemical cycling process [17, 20]. Moreover, the octahedral morphology enhances the structure stability by suppressing the manganese dissolution [22, 26, 27]. The above positive function contributes to the good electrochemical performance of $\text{LiSi}_{0.05}\text{Mn}_{1.95}\text{O}_4$ octahedrons.

Table 1 Comparison of $\text{LiSi}_{0.05}\text{Mn}_{1.95}\text{O}_4$ octahedrons and LiMn_2O_4 -based cathode materials reported by other works [17, 20, 22].

Sample	Cycling condition	Initial capacity (mAh g^{-1})	Capacity retention (%)	Reference
LiMn_2O_4 nanoparticles	1.0 C, 100 cycles	114.0	87.8	[22]
Si-doped LiMn_2O_4 particles	0.5 C, 100 cycles	134.6	85.1	[20]
$\text{LiSi}_{0.05}\text{Mn}_{1.95}\text{O}_4$ particles	1.0 C, 300 cycles	139	75	[17]
$\text{LiSi}_{0.05}\text{Mn}_{1.95}\text{O}_4$ octahedrons	1.0 C, 100 cycles	118.7	94.7%	This work

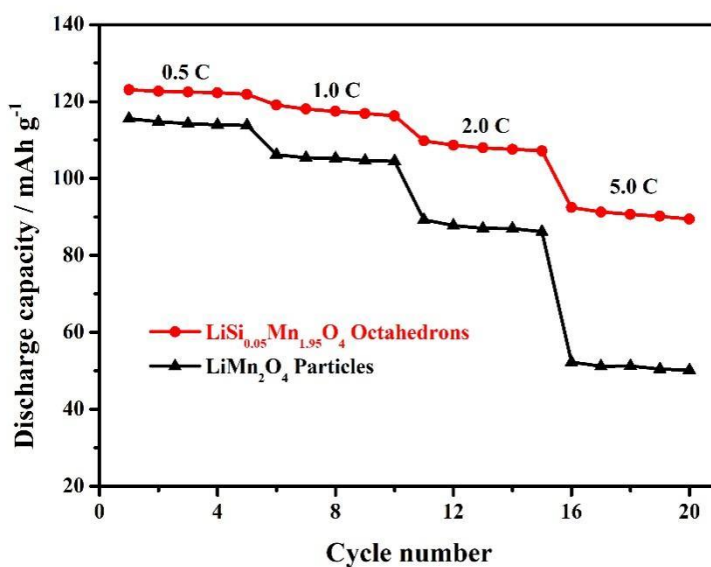


Figure 7. Rate stability of the undoped LiMn_2O_4 particles and $\text{LiSi}_{0.05}\text{Mn}_{1.95}\text{O}_4$ octahedrons.

Figure 7 presents the rate performance of the undoped LiMn_2O_4 particles and $\text{LiSi}_{0.05}\text{Mn}_{1.95}\text{O}_4$ octahedrons. It can be found that the discharge capacity is intimately connected to the cycling rate. When cycled at the low rate of 0.5 C, the discharge capacities of the undoped LiMn_2O_4 particles and $\text{LiSi}_{0.05}\text{Mn}_{1.95}\text{O}_4$ octahedrons have no obvious difference.

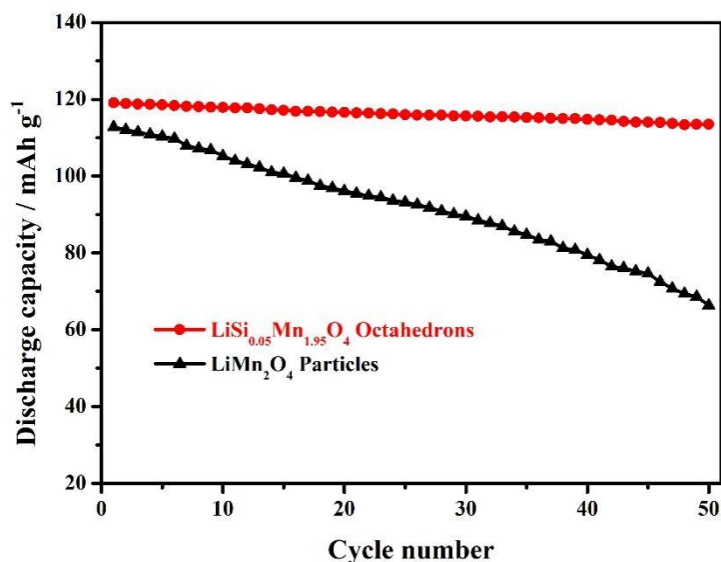


Figure 8. Cycling performance of the undoped LiMn_2O_4 particles and $\text{LiSi}_{0.05}\text{Mn}_{1.95}\text{O}_4$ octahedrons at $55\text{ }^\circ\text{C}$.

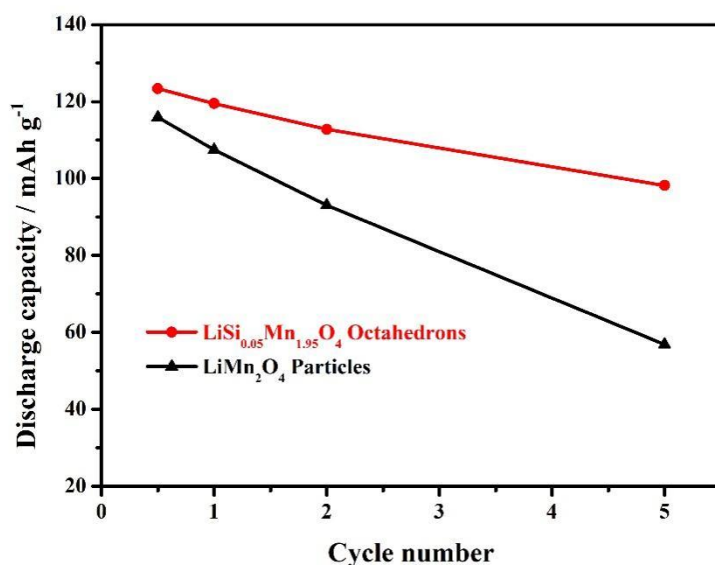


Figure 9. Rate capability of the undoped LiMn_2O_4 particles and $\text{LiSi}_{0.05}\text{Mn}_{1.95}\text{O}_4$ octahedrons at $55\text{ }^\circ\text{C}$.

However, as the cycling rate increases, the corresponding discharge capacity gradually show obvious change. When the cycling rate increases to 5.0 C , the undoped LiMn_2O_4 particles exhibit fairly small discharge capacity of 52.3 mAh g^{-1} , which is 45.2% of the initial discharge capacity of the undoped LiMn_2O_4 at 0.5 C . For the $\text{LiSi}_{0.05}\text{Mn}_{1.95}\text{O}_4$ octahedrons, the corresponding discharge capacity can reach up to 92.5 mAh g^{-1} , which is 75.1% of the initial discharge capacity of this Si-doped spinel at 0.5 C . Such good performance has much to do with the synergistic effect of Si-doping and octahedral morphology of the $\text{LiSi}_{0.05}\text{Mn}_{1.95}\text{O}_4$ octahedrons [17, 23, 27].

Figure 8 presents the cycling performance of the undoped LiMn_2O_4 particles and $\text{LiSi}_{0.05}\text{Mn}_{1.95}\text{O}_4$ octahedrons at 55 °C, and the cycling rate is set to be 1.0 C. It can be found that the combination of Si-doping and octahedral morphology performs an important role in the improvement of high-temperature electrochemical performance. The undoped LiMn_2O_4 particles exhibit poor cycling stability with lower capacity retention rate of 58.9%. For the $\text{LiSi}_{0.05}\text{Mn}_{1.95}\text{O}_4$ octahedrons, the cycling stability was significantly improved with higher discharge capacity of 113.5 mAh g^{-1} , and the corresponding capacity retention rate reaches up to 95.3%. Figure 9 shows the high-temperature rate performance of the undoped LiMn_2O_4 particles and $\text{LiSi}_{0.05}\text{Mn}_{1.95}\text{O}_4$ octahedrons at 55 °C. It can be found that the discharge capacity is intimately connected to the cycling rate. When cycled at the low rate of 0.5 C, both LiMn_2O_4 particles and $\text{LiSi}_{0.05}\text{Mn}_{1.95}\text{O}_4$ octahedrons present similar discharge capacities (115.9 mAh g^{-1} and 123.4 mAh g^{-1}). When the cycling rate increases to 5.0 C, the discharge capacity of the undoped LiMn_2O_4 particles rapidly decreases to 56.9 mAh g^{-1} . For the $\text{LiSi}_{0.05}\text{Mn}_{1.95}\text{O}_4$ octahedrons, the corresponding discharge capacity can reach up to 98.2 mAh g^{-1} . The above result further confirms the positive function of Si-doping and octahedral morphology on the electrochemical performance LiMn_2O_4 .

4. CONCLUSIONS

The $\text{LiSi}_{0.05}\text{Mn}_{1.95}\text{O}_4$ octahedrons were prepared by high-temperature solid-state method with Mn_3O_4 octahedrons as manganese precursor and SiO_2 nanoparticles as silicon dopant. The co-modification strategy of Si-doping and octahedral morphology effectively enhances the electrochemical performance of LiMn_2O_4 . The research result indicated that the Si-doping could provide more expanded and regular MnO_6 octahedrons, which achieved the good accommodation of Mn(III)–Mn(IV) interconversion during the electrochemical cycling process. Moreover, the octahedral morphology enhanced the structure stability by suppressing the manganese dissolution. The $\text{LiSi}_{0.05}\text{Mn}_{1.95}\text{O}_4$ octahedrons exhibited good cycling stability and rate performance, which may promote the widespread use of LiMn_2O_4 .

ACKNOWLEDGMENTS

This work was financially supported by the Natural Science Foundation of Henan Province (No. 202300410163) and University Students' Innovation and Pioneering Project of Henan Province (No. S202110467037X).

References

1. Q. Liu, Q. Liang, J. Guo, M. Xiang, W. Bai, H. Bai and X. Liu, *Ceram. Int.*, 47 (2021) 2441.
2. H. Liu, M. Li, M. Xiang, J. Guo, H. Bai, W. Bai and X. Liu, *J. Colloid Interface Sci.*, 585 (2021) 729.
3. R. Chen, B. Wen, H. Li, M. Xiang, C. Su, J. Guo, W. Bai and Z. Sa, *Vacuum*, 187 (2021) 110077.
4. H. Zhao, F. Li, X. Bai, T. Wu, Z. Wang, Y. Li and J. Su, *Materials (Basel)*, 11 (2018).
5. H. Zhao, D. Li, Y. Wang, F. Li, G. Wang, T. Wu, Z. Wang, Y. Li and J. Su, *Materials (Basel)*, 11 (2018) 1455.

6. Q. Ran, H. Zhao, Y. Hu, S. Hao, J. Liu, H. Li and X. Liu, *Journal of Alloys and Compounds*, 834 (2020).
7. S. Wang, M. Xiang, Y. Lu, J. Guo, C. Su, H. Bai and X. Liu, *J. Mater. Sci-Mater. El.*, 31 (2020) 6036.
8. J. Zhu, Q. Liu, M. Xiang, J. Guo, H. Bai, X. Liu, C. Su and W. Bai, *Ceram. Int.*, 46 (2020) 14516.
9. J. Guo, Y. Chen, C. Xu, Y. Li, S. Deng, H. Xu and Q. Su, *Ionic*, 25 (2019) 2977.
10. J. Cao, S. Guo, R. Yan, C. Zhang, J. Guo and P. Zheng, *J. Alloy. Compd.*, 741 (2018) 1.
11. H. Zhao, F. Li, X. Liu, C. Cheng, Z. Zhang, Y. Wu, W. Xiong and B. Chen, *Electrochim. Acta*, 151 (2015) 263.
12. H. Zhao, F. Li, X. Liu, W. Xiong, B. Chen, H. Shao, D. Que, Z. Zhang and Y. Wu, *Electrochim. Acta*, 166 (2015) 124.
13. H. Zhao, S. Liu, Z. Wang, Y. Cai, M. Tan and X. Liu, *Electrochim. Acta*, 199 (2016) 18.
14. J. Hao, H. Bai, J. Liu, F. Yang, Q. Li, C. Su and J. Guo, *Journal of Alloys and Compounds*, 668 (2016) 200.
15. D. Zhan, Q. Zhang, X. Hu, G. Zhu and T. Peng, *Solid State Ionics*, 239 (2013) 8.
16. Y. Fu, H. Jiang, Y. Hu, Y. Dai, L. Zhang and C. Li, *Ind. Eng. Chem. Res.*, 54 (2015) 3800.
17. A. Iturrondobeitia, A. Goñi, V. Palomares, I. Gil de Muro, L. Lezama and T. Rojo, *J. Power Sources*, 216 (2012) 482.
18. L. Xiong, Y. Xu, C. Zhang, Z. Zhang and J. Li, *J. Solid State Electr.*, 15 (2010) 1263.
19. W. Wen, B. Ju, X. Wang, C. Wu, H. Shu and X. Yang, *Electrochimica Acta*, 147 (2014) 271.
20. H. Zhao, S. Liu, Z. Wang, Y. Cai, M. Tan and X. Liu, *Ceram. Int.*, 42 (2016) 13442.
21. H. Zhao, Y. Nie, Y. Li, T. Wu, E. Zhao, J. Song and S. Komarneni, *Ceram. Int.*, 45 (2019) 17183.
22. Q. Zhang, J. Mei, X. Wang, J. Guo, F. Tang and W. Lu, *Journal of Alloys and Compounds*, 617 (2014) 326.
23. Y. Li, G. Zhu, Q. Ran, J. Liu, Y. Zhou, M. Zhao, P. Cao and H. Zhao, *International Journal of Electrochemical Science*. 16 (2021) 210933.
24. H. Zhao, X. Liu, C. Cheng, Q. Li, Z. Zhang, Y. Wu, B. Chen and W. Xiong, *J. Power Sources*. 282 (2015) 118.
25. H. Zhao, Y. Nie, D. Que, Y. Hu and Y. Li, *Materials (Basel)*, 12 (2019) 2807.
26. Y. Cai, Y. Huang, X. Wang, D. Jia, W. Pang, Z. Guo, Y. Du and X. Tang, *J. Power Sources*. 278 (2015) 574.
27. G. Jin, H. Qiao, H. Xie, H. Wang, K. He, P. Liu, J. Chen, Y. Tang, S. Liu and C. Huang, *Electrochim. Acta*, 150 (2014) 1.